GEOLOGY

Remnants of Eoarchean continental crust derived from a subducted proto-arc

Rongfeng Ge,[1,2]* Wenbin Zhu,[1]* Simon A. Wilde,[2] Hailin Wu[1]

Eoarchean [3.6 to 4.0 billion years ago (Ga)] tonalite-trondhjemite-granodiorite (TTG) is the major component of Earth's oldest remnant continental crust, thereby holding the key to understanding how continental crust originated and when plate tectonics started in the early Earth. TTGs are mostly generated by partial melting of hydrated mafic rocks at different depths, but whether this requires subduction remains enigmatic. Recent studies show that most Archean TTGs formed at relatively low pressures (≤1.5 GPa) and do not require subduction. We report a suite of newly discovered Eoarchean tonalitic gneisses dated at ~3.7 Ga from the Tarim Craton, northwestern China. These rocks are probably the oldest high-pressure TTGs so far documented worldwide. Thermodynamic and trace element modeling demonstrates that the parent magma may have been generated by water-fluxed partial melting of moderately enriched arc-like basalts at 1.8 to 1.9 GPa and 800° to 830°C, indicating an apparent geothermal gradient (400° to 450°C GPa^{-1}) typical for hot subduction zones. They also locally record geochemical evidence for magma interaction with a mantle wedge. Accordingly, we propose that these high-pressure TTGs were generated by partial melting of a subducted proto-arc during arc accretion. Our model implies that modern-style plate tectonics was operative, at least locally, at ~3.7 Ga and was responsible for generating some of the oldest continental nuclei.

INTRODUCTION

Tonalite-trondhjemite-granodiorite (TTG) are sodic granitoids that constitute most of the Archean continental crust, but they diminish over time and give way to high-potassium (K) calc-alkaline granitoids in post-Archean crustal domains (1–4). Thus, their origin and secular evolution are crucial to understanding the origin and evolution of continental crust. TTGs have distinct geochemical signatures, including high Na_2O/K_2O ratios and high strontium (Sr) contents, low heavy rare earth element (REE) and yttrium (Y) contents, and depletion of niobium (Nb), tantalum (Ta), and titanium (Ti) (1–4). It is generally agreed that TTGs were mostly produced by partial melting of hydrated mafic rocks with various amounts of garnet, clinopyroxene, amphibole, and rutile, but little or no plagioclase in the residue, at depths corresponding to at least 0.8 to 1 GPa (1–4). However, in what geodynamic environment this deep melting occurred is highly controversial. Proposed models include melting of subducted oceanic slabs (5, 6) or oceanic plateaus (7), thickened oceanic plateaus (8–10), or thickened oceanic arcs (11, 12). Recently, Moyen (13) showed that much of the controversy probably arises from lumping together of TTGs with diverse compositions that formed at different melting pressures. Most sodic TTGs (~80%) belong to the medium-pressure (MP) and low-pressure (LP) subgroups that likely formed in the lower crust in equilibrium with garnet amphibolites or high-pressure mafic granulites, with various amounts of plagioclase in the residue. Only ~20% of sodic TTGs belong to the high pressure (HP) subgroup, derived from rutile-bearing eclogites with abundant garnet and rutile but no plagioclase in the residue, possibly in subduction zones (13). Therefore, identification of HP TTGs in early Archean geological records and understanding their petrogenesis have the potential to determine when plate tectonics started and how continental crust formed in the early Earth.

Eoarchean TTGs have been identified in several gneiss complexes around the world (Fig. 1A), but they mostly occur as small tectonic enclaves in younger rocks and only occupy about 1 millionth of Earth's surface (14). Moreover, because of multiple episodes of high-grade metamorphism, partial melting, and ductile deformation, most Eoarchean TTGs record multiple age components even in a single sample, resulting in mixed whole-rock geochemical compositions. Recently, pristine compositions have been reported for samples with single magmatic ages from relatively low-strain zones in the ~3.7 to 3.9 Ga (billion years ago) Itsaq Complex (Greenland) (12, 15, 16), the ~3.9 to 4.0 Ga Acasta Complex (Canada) (17, 18), and the ~3.8 Ga Anshan Complex (North China) (19, 20) (see table S4 for a more complete reference list). These data suggest that most Eoarchean TTGs are LP or MP TTGs that were likely derived from partial melting of variably thickened mafic lower crust (11, 12, 16). Alternatively, shallow assimilation and fractional crystallization (AFC) of mafic magma in an Iceland-like setting has been proposed for a group of ~4.02 Ga high-FeO^T tonalites from the Acasta Complex (18). Although enriched, arc-like basalts have been suggested as the source of TTGs from the Itsaq Complex (11, 12, 16), the generation of the LP and MP TTGs itself did not require subduction, thus questioning the operation, scale, and style of plate tectonics in the early Archean. Here, we report a suite of newly identified Eoarchean (~3.7 Ga) tonalitic gneisses that are compositionally similar to HP TTGs from the Tarim Craton of northwestern China. Pristine whole-rock compositions of these rocks are compared with data from Itsaq, Acasta, and Anshan to evaluate the geodynamic processes that generated the first continental crust on Earth.
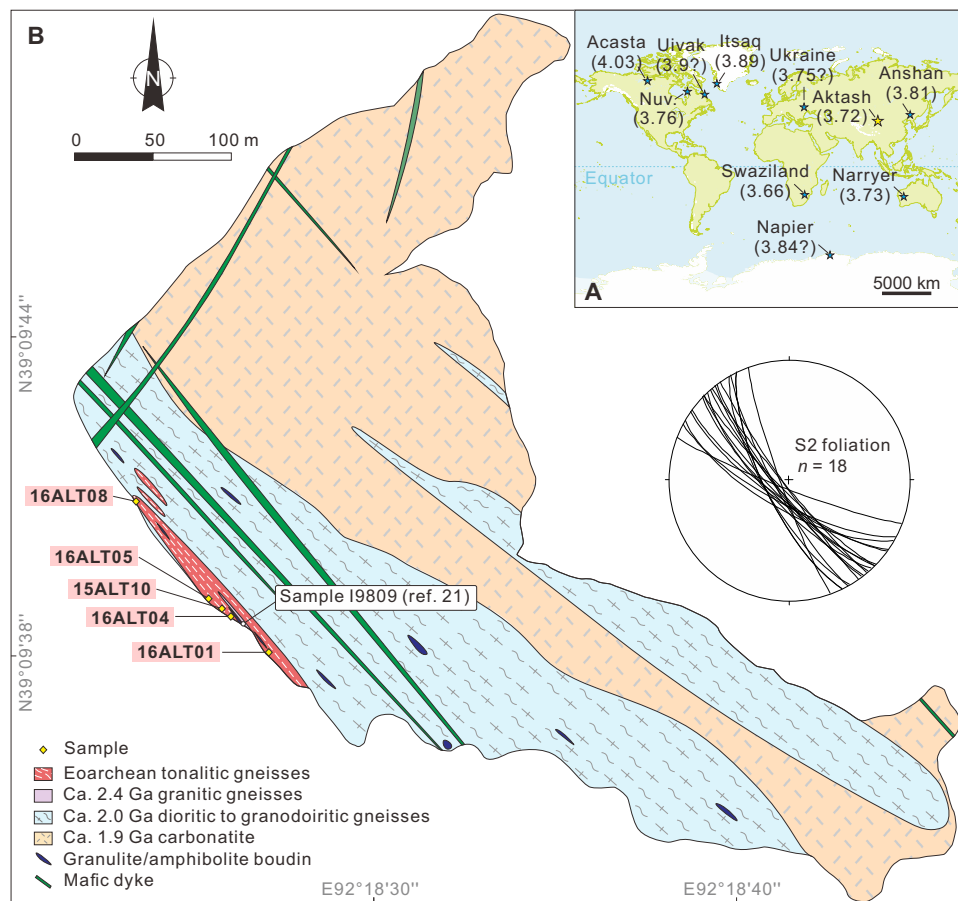
RESULTS

Eoarchean Aktash gneiss complex

Eoarchean TTG gneisses were identified from the Aktash Tagh area in the southeastern margin of the Tarim Craton, northwestern China (figs. S1 to S4) (21). Detailed mapping shows that they occur as small tectonic enclaves in Paleoproterozoic (~2.0 to 2.1 Ga) dioritic to granodioritic gneisses, with the largest being ~150 m long and 10 to 20 m wide (Fig. 1B). They contain lenses of mafic granulite/amphibolite and high-K granitic gneiss, the latter being dated to ~2.4 Ga and found to

Fig. 1. Location and geological map of the Eoarchean Aktash gneisses complex. (**A**) Global distribution of Eoarchean gneiss complexes and their oldest TTG components (ages in Ga). Nuv., Nuvvuagittuq. (**B**) Geological map of the Aktash Complex. The Eoarchean gneisses occur as tectonic enclaves in ~2.0-Ga gneisses. The inset shows the lower hemisphere equal-area stereoprojection of the regional foliation (S2) at the outcrop. See the Supplementary Materials and fig. S1 for detailed regional geological setting.

contain Eoarchean inherited zircons (*21*). These rocks were all metamorphosed to granulite facies at ~2.0 Ga and were affected by partial melting and multiple episodes of ductile deformation. They were intruded by ~1.9 Ga carbonatites and ~1.8 Ga granitic veins and mafic dykes.

Five samples were dated by in situ zircon U-Pb techniques (see Materials and Methods). They yield similar zircon populations (Fig. 2A) and U-Pb age patterns (fig. S4), which are summarized in Fig. 2B. Zircon cathodoluminescence (CL) images reveal complex internal structures, with oscillatory zoned magmatic cores surrounded by multiple gray to dark recrystallized mantles, which are commonly separated by a bright seam from multiple metamorphic rims (Fig. 2A). U-Pb isotopic data (tables S1 and S2) show that the concordant ages from the core and mantle domains spread along concordia from ~3.55 to 3.75 Ga. Except for one analysis with an apparent age of 3745 ± 12 Ma (million years ago, 2σ) that possibly records an inherited age, the oldest concordant ages of the magmatic cores record a weighted mean ^{207}Pb/^{206}Pb age of 3713 ± 8 Ma [mean square weighted deviation (MSWD) = 1.4, *n* = 7; Fig. 2B]. This is consistent within error with the weighted mean ^{207}Pb/^{206}Pb ages and upper intercept ages (3.68 to 3.72 Ga) for individual samples and is interpreted as the best estimate of the magmatic crystallization age of the protolith of the Eoarchean Aktash gneiss. The youngest concordant ages of the recrystallized mantles define a weighted mean ^{207}Pb/^{206}Pb age of 3561 ± 9 Ma (MSWD = 0.71, *n* = 10; Fig. 2B),

which is interpreted as the time of metamorphic recrystallization of the primary magmatic zircons. The remaining analyses plot along or below the concordia curve, reflecting the multiple and/or incomplete radiogenic Pb (Pb*) loss. The metamorphic rims are dated at ~2.0 Ga, consistent with the zircon ages of adjacent high-grade metamorphic rocks in the area (*21*).

In situ zircon Hf isotopic analysis (see Materials and Methods) shows that the cores and mantles have similar, although slightly heterogeneous, ^{176}Hf/^{177}Hf ratios (Fig. 2C and table S3), consistent with the recrystallization origin of the latter. Moreover, the young, discordant analyses have indistinguishable ^{176}Hf/^{177}Hf ratios from the oldest grains, supporting the interpretation of Pb* loss (*22*). When calculated using the magmatic crystallization age, the εHf values form a normal distribution with a mean value of −0.7 ± 2.6 (2σ), consistent with a magma source derived from a near chondritic mantle, as commonly found for other Eoarchean TTGs (*22*).

Whole-rock geochemical data (see Materials and Methods and table S4) show that most samples have consistent major and trace element compositions, and good correlations exist between relatively immobile elements, suggesting that most elements (except for Th, U, Rb, and Ba) were not significantly mobilized by later high-grade metamorphism, migmatization, or alteration (fig. S5). These samples have a tonalitic composition, except for sample 16ALT08-3 with high K$_2$O
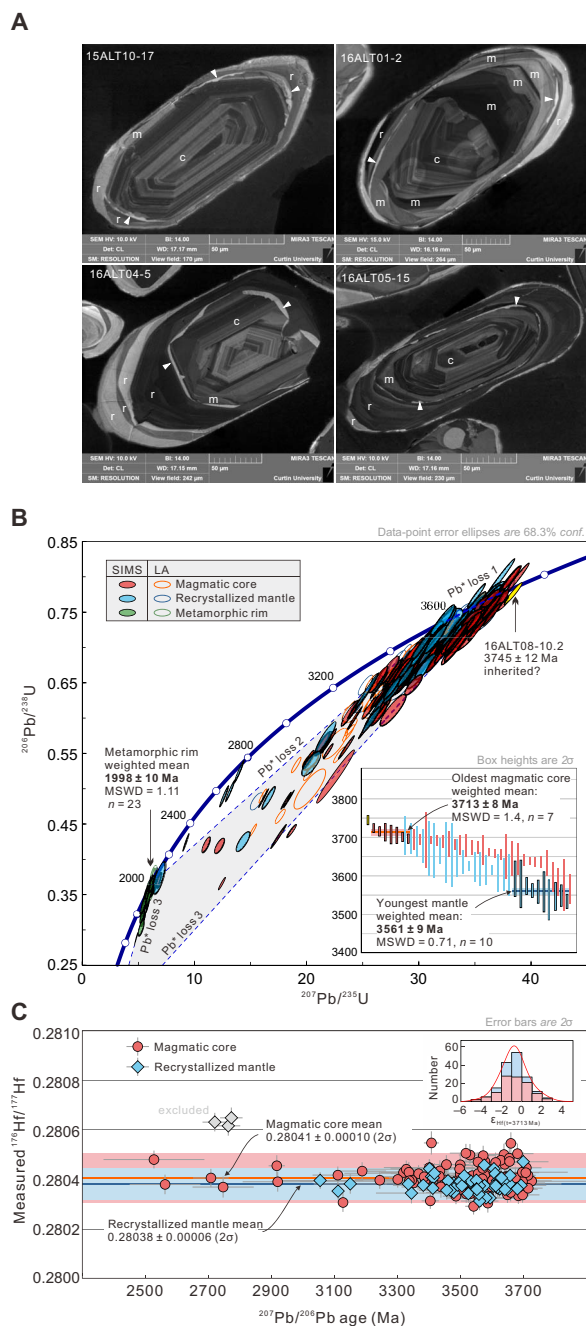
Fig. 2. Zircon structures, U-Pb ages, and Hf isotopic compositions of the Eoarchean Aktash tonalitic gneisses. (**A**) Representative CL images showing complex core (c), mantle (m), and rim (r) structures. Oscillatory zoned magmatic cores are surrounded by multiple recrystallized mantles that are separated by a thin bright seam (white arrows) with multiple metamorphic overgrowth rims. (**B**) Concordia diagram showing all U-Pb ages by secondary ion mass spectrometer (SIMS) and laser ablation (LA) (see Materials and Methods). The inset shows the $^{207}Pb/^{206}Pb$ ages of concordant analyses from magmatic cores and recrystallized mantles, with weighted mean ages of the oldest cores and youngest mantles interpreted as the best estimates of magma crystallization and metamorphic recrystallization, respectively. Other discordant analyses plot in the region defined by multiple radiogenic Pb (Pb*) loss events. (**C**) Measured $^{176}Hf/^{177}Hf$ ratios versus $^{207}Pb/^{206}Pb$ ages for the magmatic cores and recrystallized mantles, showing the indistinguishable Hf isotopic compositions for both domains that do not change with apparent ages. The inset shows the near Gaussian distribution of εHf values calculated using the magmatic crystallization age.

that plots in the granite field (Fig. 3A). The tonalite samples have trace element characteristics typical of Archean TTGs, including high Sr, low Y, and heavy REE. Compared to the Eoarchean TTGs from the Itsaq, Acasta, and Anshan complexes, the Aktash samples have higher Sr [476 to 747 ppm (parts per million)], lower Y (1.9 to 7.0 ppm), and heavy REE contents (Yb = 0.17 to 0.56 ppm), and thus higher Sr/Y (82 to 282) and normalized La/Yb (32.0 to 136) and Gd/Yb (2.59 to 6.88) ratios (Fig. 3B and Table 1). Moreover, these samples have very low Nb (average, 2.8 ppm), Ta (average, 0.10 ppm), and Ti [average, 0.46 weight % (wt %)] contents relative to other Eoarchean TTGs (Fig. 3C). These geochemical features are consistent with those for HP TTGs (13), whereas samples from the Itsaq, Acasta, and Anshan complexes mostly plot in the MP and LP TTG fields (Fig. 3, B and C, and Table 1), indicating that the Aktash tonalites were probably derived from higher pressures. In addition, the Aktash samples tend to have lower SiO_2 (as low as 57 wt %) but higher MgO (up to 4.71 wt %), Cr (up to 122 ppm), and Ni (up to 121 ppm) contents, and higher Mg# (up to 60.1) than the other Eoarchean TTGs and experimentally derived TTG melts, with the most mafic sample (16ALT04-2) plotting close to the average low-SiO_2 adakite and sanukitoid (3) (Fig. 3D).

Thermodynamic and trace element modeling

It is generally agreed that Archean TTGs were generated by partial melting of hydrated mafic rocks (1–4). Although an AFC origin has been proposed for the ~4.02 Ga high-FeO^T tonalites in the Acasta Complex (18) and for some TTG-like plutons in Phanerozoic arcs (23), this model is not favored for most Archean TTGs because both intermediate products (for example, gabbro and diorite) and cumulates (for example, garnetite and hornblendite) of fractional crystallization are rare or absent in Archean geological records. This also applies to the Aktash tonalites, the composition of which was likely controlled by progressive partial melting and subsequent interaction with mantle peridotite (see the Supplementary Materials). In the partial melting model, the primary magma composition is controlled by source composition and melting conditions (for example, pressure, temperature, and water activity), which are likely related to tectonic settings. Here, we compiled a database of mafic rocks from modern oceanic settings (mid-ocean ridges, oceanic plateaus, and oceanic arcs) and Archean cratons (see Materials and Methods and table S7) to evaluate the tectonic setting that generated Eoarchean TTGs and thus Earth's oldest continental crust.

Simple batch melting modeling using the highly incompatible large-ion lithophile elements (LILEs; for example, Rb, Ba, Th, U, and K) provides important constraints on the source of TTGs (Fig. 4A and fig. S7). Although these elements can be mobile during alteration and metamorphism, the global average tends to eliminate this effect. Our compilation shows that TTGs are significantly enriched in LILEs relative to modern mid-ocean ridge basalts (MORB; Fig. 4A and table S6). This enrichment is independent of age and melting pressure and is probably a reflection of source composition and degree of partial melting. Our results confirm that, for 10 to 30% partial melting, MORB is too depleted in LILEs to produce TTGs (Fig. 4A) (7, 9). Oceanic plateau basalts (OPB) have been considered as the source of TTGs (7, 8) because they are derived from relatively enriched mantle plumes (24). However, our results show that most modern OPB are dominated by tholeiites that are only marginally more enriched (some are even more depleted) than modern MORB, which is insufficient to produce the enrichment seen in TTGs unless a very low degree (<7%) of partial melting is involved. This is consistent with a recent experimental finding that addition of K_2O-rich fluids is needed to make TTGs from primitive OPB (25). More enriched
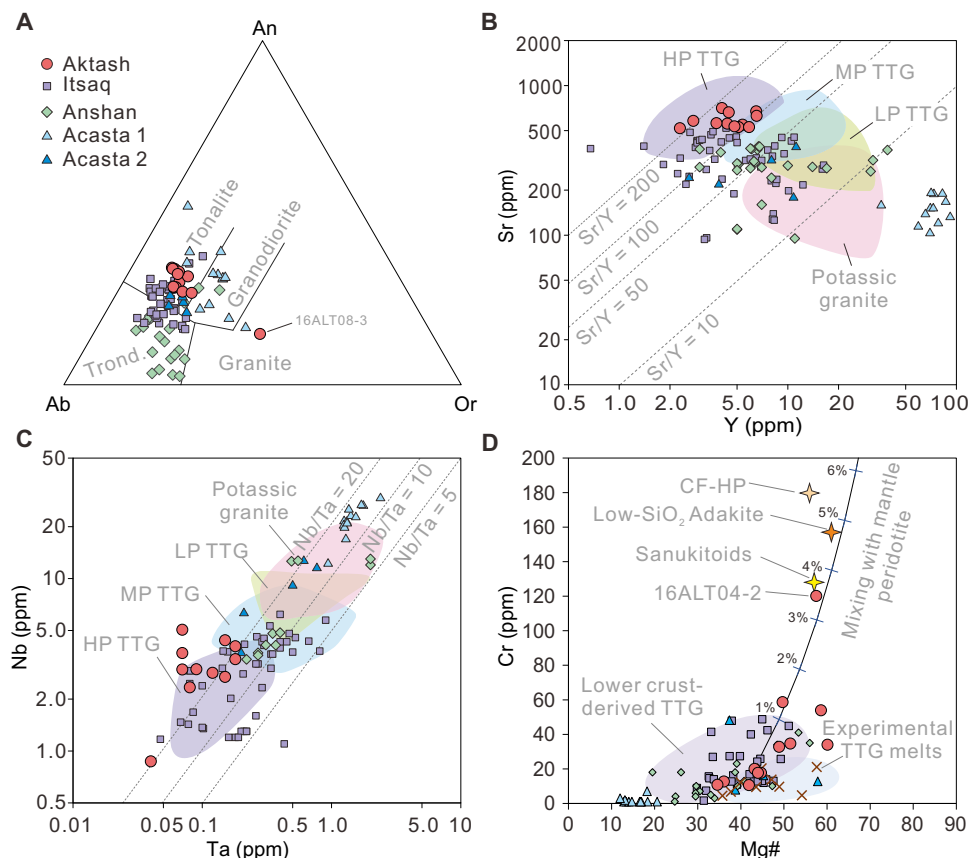
Fig. 3. Geochemical composition of the Eoarchean Aktash tonalitic gneisses compared to Eoarchean TTGs from the Itsaq, Acasta, and Anshan gneiss complexes. Average compositions of individual samples from replicate analyses are used in the plots for the Aktash gneisses. Acasta 1 refers to the 4.02-Ga high-FeO[T] tonalites that are compositionally different from typical TTGs. See table S4 for data source. (**A**) Feldspar triangular classification diagram showing the tonalitic composition of the studied samples, except for sample 16ALT08-3. (**B**) Sr/Y diagram. (**C**) Nb/Ta diagram. The Aktash tonalitic gneisses mostly plot into the HP TTG fields in (B) and (C), whereas other Eoarchean TTGs mostly plot into the medium and LP TTG fields (13). (**D**) Cr/Mg# diagram showing the higher Cr contents and Mg# of the Aktash tonalitic gneisses relative to the lower crust–derived Eoarchean TTGs and experimental TTG melts (37). The most "mafic" sample (16ALT04-2) plots close to the average low-SiO$_2$ Adakites and Archean Sanukitoids (3), which can be modeled by simple mixing with 3 to 5% mantle peridotite (DP1) (39). This provides a minimum constraint for mantle peridotite interacted with TTG melts because experiments show that this interaction produces peritectic mafic minerals (for example, garnet and pyroxene) that host most of the MgO, Cr, and Ni, so that even interaction with 30% peridotite produces melts (for example, CF-HP) similar to our most mafic sample (39).

basalts do exist in oceanic plateaus and oceanic islands, but their restricted abundance and need for selective melting is a problem when large volumes of TTGs are to be produced. The only mafic rocks enriched enough to be the source of extensive TTGs in a modern oceanic setting are island arc basalts (IAB; Fig. 4A and fig. S7). In fact, the average composition of modern IAB is slightly too enriched in K$_2$O, which, under similar degrees of partial melting, would produce melts that tend to be K-rich granodiorite to granite (Fig. 4A and fig. S7), a conclusion supported by partial melting experiments (26).

The tectonic setting of Archean basalts is a subject of considerable debate, and unambiguous geological records of Archean MORB and OPB are rare or absent (27). Although the Archean mantle may not be as depleted as it is today, the mantle-derived melts tend to be diluted by higher-degree partial melting due to higher Archean mantle potential temperature (28, 29). The net result is that Archean MORB and OPB may not be significantly enriched than modern counterparts. By contrast, moderately enriched tholeiitic basalts have been documented in the Eoarchean Isua (30–32) and Nuvvuagittuq (33) greenstone belts. These rocks have trace element patterns and lithological associations (for example, tholeiite-boninite association) remarkably similar to those

found in modern oceanic arcs and have been interpreted as formed in Eoarchean proto-arcs (14, 33, 34). Recent geochemical (11, 12, 16) and experimental (35) studies have demonstrated that these Eoarchean arc-like tholeiites are a suitable source for the Eoarchean TTGs in these localities. These results imply that most TTGs probably require a moderately enriched mafic source related to some form of crustal recycling in arc-like settings as early as the Eoarchean and that the secular evolution from TTGs to high-K granodiorite-granite may be partly ascribed to secular enrichment of arc-related basalts in addition to enhanced intracrustal reworking (2, 4).

To further constrain the pressure (P)–temperature (T) conditions and source water content [X(H$_2$O)] under which Archean TTGs were derived, thermodynamic partial melting modeling was performed for the median composition of arc-like basalts (Th/Nb >0.1) (27) from Archean cratons (see Materials and Methods and table S7). Note that these basalts have a wide range of trace element compositions and not all of them were necessarily generated in arcs considering continental contamination and uncertainties in tectonic interpretations (27). However, this median composition appears to be representative of the least altered, moderately enriched high-aluminum arc-like

Table 1. Median values of key elemental concentrations and ratios for TTGs and selected modeled melts. See tables S4, S6, S7, and S9 for details.

	K$_2$O (wt %)	Rb (ppm)	Sr (ppm)	Y (ppm)	Sr/Y	Nb (ppm)	Nb/Ta	Mg#
TTGs derived from different depths								
LP TTG	1.67	68.1	277	14.0	20.5	8.00	10.6	37.7
MP TTG	1.53	52.0	443	7.61	57.6	5.00	10.9	41.5
HP TTG	1.52	40.0	576	3.83	130	2.41	13.3	42.5
Eoarchean TTGs								
Itsaq	1.42	50.3	327	4.79	57.2	3.11	12.2	42.4
Anshan	1.89	111	295	6.50	47.2	4.12	13.3	33.7
Acasta (group 2)	1.76	43.8	241	8.00	37.1	9.10	18.4	42.0
Aktash	1.48	22.8	561	4.46	127	2.97	23.0	48.9
Selected modeled TTG melts of Archean arc-like basalts [X(H$_2$O) = 2.5 wt %]								
T = 820℃, P = 0.6 GPa	1.11	29.3	218	14.0	15.6	8.54	18.8	30.2
T = 820℃, P = 1.0 GPa	1.24	33.6	304	9.94	30.5	6.40	18.1	33.6
T = 820℃, P = 1.4 GPa	1.27	33.1	430	5.85	73.5	3.35	16.7	37.8
T = 820℃, P = 1.9 GPa	1.43	34.0	616	4.53	136	2.32	16.0	47.5

tholeiites in the Isua greenstone belt (30–32) and appears to be a suitable source of TTGs in terms of LILE concentrations (Fig. 4A). Thermodynamic calculations were carried out using the newly calibrated solution models for tonalitic melt, amphibole, and clinopyroxene (see Materials and Methods) (36). We calculated P-T and T-X(H$_2$O) phase diagrams (fig. S8), as well as mineral assemblage and degree of partial melting at ~1500 discrete points (table S9) with P-T-X(H$_2$O) conditions ranging from 750° to 950°C, 0.6 to 2.0 GPa, and 1.0 to 3.0 wt %, respectively. The latter were then used to calculate the major and trace element composition of the modeled melts (see Materials and Methods and table S9) (10–12). Our results indicate that Sr contents and Sr/Y ratios, as well as Nb-Ta and heavy REE contents, of the modeled melts are sensitive to melting pressures, whereas LILE (for example, K and Rb) and light REE contents are controlled by melting temperature and source water content (and thus degree of partial melting; Fig. 5 and fig. S8). These geochemical parameters of the modeled melts were fitted with the observed compositions of the Eoarchean TTGs to estimate the optimum P-T-X(H$_2$O) conditions from which their parent magmas were derived. The results show that the median composition of the Aktash tonalites is best matched by melts generated by 15 to 20% melting at relatively high pressure (1.8 to 1.9 GPa) and low temperature (800° to 830°C) conditions when 2 to 3 wt % water is present in the source (Figs. 4B and 5, and Table 1). Melting at variably lower pressures (for example, 0.6 to 1.4 GPa; Fig. 4B and Table 1) fails to reproduce the high Sr and Sr/Y, as well as the low Nb-Ta and heavy REE contents. In a relatively dry system (1 to 1.5 wt % H$_2$O), similar degrees of partial melting can be achieved at higher temperatures (900° to 950°C) at 1.8 to 1.9 GPa, but the resultant melts have slightly higher light REE contents than the observed median values (Fig. 4B). The average TTGs from the Itsaq and Anshan complexes can be generated from the same source but at relatively lower pressures (1.0 to 1.5 GPa; fig. S9), consistent with previous studies of the Itsaq Complex

(11, 12). A good fit was also obtained for melting at low temperature (750° to 810°C) with high water contents (2 to 3 wt %), although high temperature melting with lower initial water contents (1 to 1.5 wt %) cannot be completely ruled out considering the large compositional ranges of each suite (fig. S9). The relatively low Sr and high heavy REE and Y contents of a few TTG samples from the Acasta gneisses suggest a melting pressure of ~1.0 GPa, but their relatively high light REE contents probably require a more enriched source (fig. S9).

DISCUSSION

The above modeling suggests that most Eoarchean TTGs (Itsaq and Anshan) are MP and LP TTGs that were likely generated by partial melting in the garnet amphibolite to HP granulite facies (Fig. 5), most likely in the lower crust of thickened proto-arcs (1.0 to 1.5 GPa). This is consistent with the results of recent geochemical (11, 12, 16), experimental (37), and thermodynamic studies (10, 38). However, the Aktash samples are similar to HP TTGs and can only be generated by partial melting of rutile-bearing eclogites with no plagioclase and minor or no amphibole in the residue at 1.8 to 1.9 GPa, or ~60 km depth. This significantly exceeds the crustal thickness of modern oceanic arcs and oceanic plateaus and is probably also difficult to achieve for early Archean crust, which was probably rheologically weak due to higher mantle potential temperature and would be gravitationally unstable (delaminated) at the base once thickened to 40 to 50 km (29). Therefore, melting of thickened mafic lower crust can be ruled out for the Aktash tonalites. The relatively high Mg# and Cr and Ni contents of the most mafic sample also imply melting at mantle depths and interaction with at least 3 to 5% mantle peridotites (Fig. 3D) (1, 3, 4, 39); interaction with ultramafic rocks (for example, komatiite) at shallow crustal levels is unlikely because our thermodynamic modeling (unpublished) indicates that this would produce peritectic plagioclase and orthopyroxene that tend to
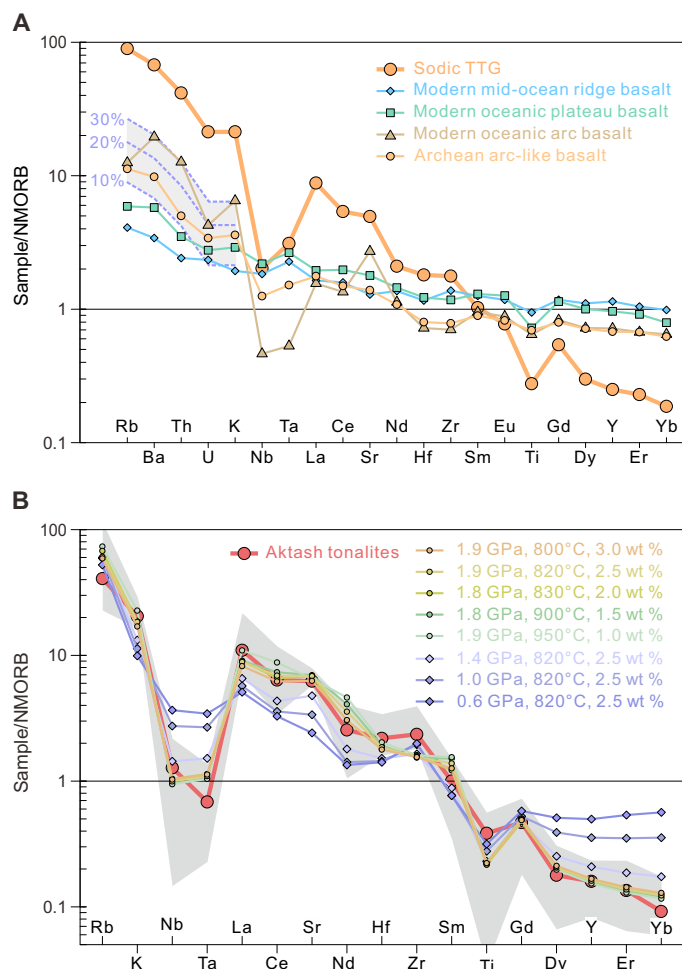
Fig. 4. Trace element modeling. (A) Trace element patterns for the median composition of TTGs (13) and their potential source rocks (tables S6 and S7), highlighting the significant enrichment of LILEs (for example, Rb, Ba, Th, U, and K) in TTGs. The dashed lines represent the degree of LILE enrichment required for the source to produce TTGs by 10, 20, or 30% melting, assuming perfect incompatibility (bulk partition coefficient = 0). In modern oceanic settings, only IAB are enriched enough to be the source of TTGs; mid-ocean ridge and oceanic plateau basalts are too depleted. The median composition of Archean arc-like basalts used for thermodynamic modeling appear to be a suitable source of TTGs. NMORB, normal MORB. **(B)** Trace element patterns of TTG melts calculated at different P-T-$X(H_2O)$ conditions for the median composition of Archean arc-like basalts (table S9). The shaded area shows the overall compositional range of the ~3.7 Ga Aktash tonalites. The best fit for the median composition of the Aktash tonalites is obtained for water-fluxed melting [$X(H_2O) = 2$ to 3 wt %] at 1.8 to 1.9 GPa and 800° to 830°C; dehydration melting [$X(H_2O) = 1.0$ to 1.5 wt %] at higher temperatures (900° to 950°C) results in a poorer fit in light REE. Melts derived from lower pressures at 1.4, 1.0, and 0.6 GPa significantly deviate from the median Aktash tonalites in terms of Nb-Ta, Sr and Y, and heavy REE contents.

eliminate the characteristic trace element features of TTGs (for example, high Sr and Sr/Y).

Whether this deep melting occurred in subduction zones or delaminated lower crust requires further discussion. One difference between these two scenarios may lie in the melting temperature (and thus apparent thermal gradient) and water activity. Partial melting in subduction zones may occur at relative low temperatures due to high water contents derived from dehydration of subducted slabs and overlying

sediments, whereas delaminated lower crust is relatively dry and can only be melted by conductive heating due to high thermal gradients (>750°C GPa^{-1}) (10, 29). Thermodynamic and trace element modeling shows that the Aktash tonalites were most likely generated by low-temperature (800° to 830°C) melting when 2 to 3 wt % water is added (Figs. 4B and 5), which exceeds the maximum water content of fully hydrated amphibolites at the solidus (~1.7 wt %; fig. S8) and thus implies at least 0.3 wt % water-fluxed melting. High-temperature (900° to 950°C) dehydration melting with low source water contents [$X(H_2O) = 1$ to 1.5 wt %] tends to yield melts that are slightly more enriched in light REE than the median Aktash tonalite, although this possibility cannot be entirely ruled out. Low-temperature water-fluxed melting is consistent with the low zircon saturation temperature (T_{Zr}) of these samples (average, 780° ± 20°C, 1σ; table S4). Because the Zr contents do not correlate with whole-rock SiO_2 (figs. S5 and S10) and an inherited zircon is present, parent magmas of these rocks were probably initially zircon saturated, thus T_{Zr} provides a reasonable estimate of primary magma crystallization temperature. Another line of evidence of low temperature, water-fluxed melting comes from the high Nb/Ta ratios (median, ~23.0) of the Aktash tonalites. Detailed experimental studies (40) demonstrate that Nb-Ta fractionation during partial melting of mafic rocks is mainly controlled by partition coefficients of rutile, which are largely dependent on temperature and source water content, and that only low temperature, water-fluxed melting can produce melts with high Nb/Ta ratios. Collectively, these results imply an apparent thermal gradient of 400° to 450°C GPa^{-1} for the Aktash tonalites (Fig. 5), which is considerably lower than that for partial melting of thickened or delaminated lower crust of Archean volcanic plateaus (10, 29) but similar to that expected for Archean hot subduction zones (5, 6). Considering the moderately enriched, arc-like basaltic source, we propose that the Aktash tonalites were likely produced by water-fluxed melting of the mafic component of an Eoarchean proto-arc that was subducted to mantle depths during its accretion or collision with another arc at ~3.7 Ga. By contrast, partial melting of the lower crust of the variably thickened overriding arc, triggered by underplating of hydrous basalts or TTG magmas, could have been responsible for generating the MP to LP TTGs from the Itsaq and Anshan complexes.

There has been considerable debate about when plate tectonics started in the early Earth. Recent studies on paired metamorphism (41), diamond inclusions (42), zircon Hf and O isotopes (43, 44), and crustal composition (45) variously suggest that plate tectonics was initiated during 2.8 to 3.2 Ga. Numerical modeling (46) demonstrates that the viability and style of subduction is mainly controlled by mantle potential temperature (T_p) in the early Earth, which is variably higher than it is today (28, 29). When T_p is 175° to 250°C higher, the lithosphere is weak, and subduction is intermittent, characterized by frequent slab breakoff, and when T_p is more than 250°C hotter, the lithosphere would be too weak to be subducted (46). Note that the Eoarchean T_p value, however, remains uncertain due to lack of petrological constraints (28, 29). Geochemical and geological evidence from the Isua (14, 34) and Nuvvuagittuq (33) greenstone belts suggest that some form of crustal recycling and terrane accretion was operative as early as 3.7 to 3.8 Ga. Our findings show that TTGs require a mafic source that was significantly enriched in fluid-mobile elements, which most likely results from water-fluxed mantle melting in arc-related settings (11, 12, 16). The Aktash tonalites require transport of these enriched basalts to mantle depths along a relatively cold geotherm, implying large-scale horizontal tectonics that were capable of transporting one arc beneath another. The inferred melt-peridotite interaction indicates the presence of a mantle wedge and
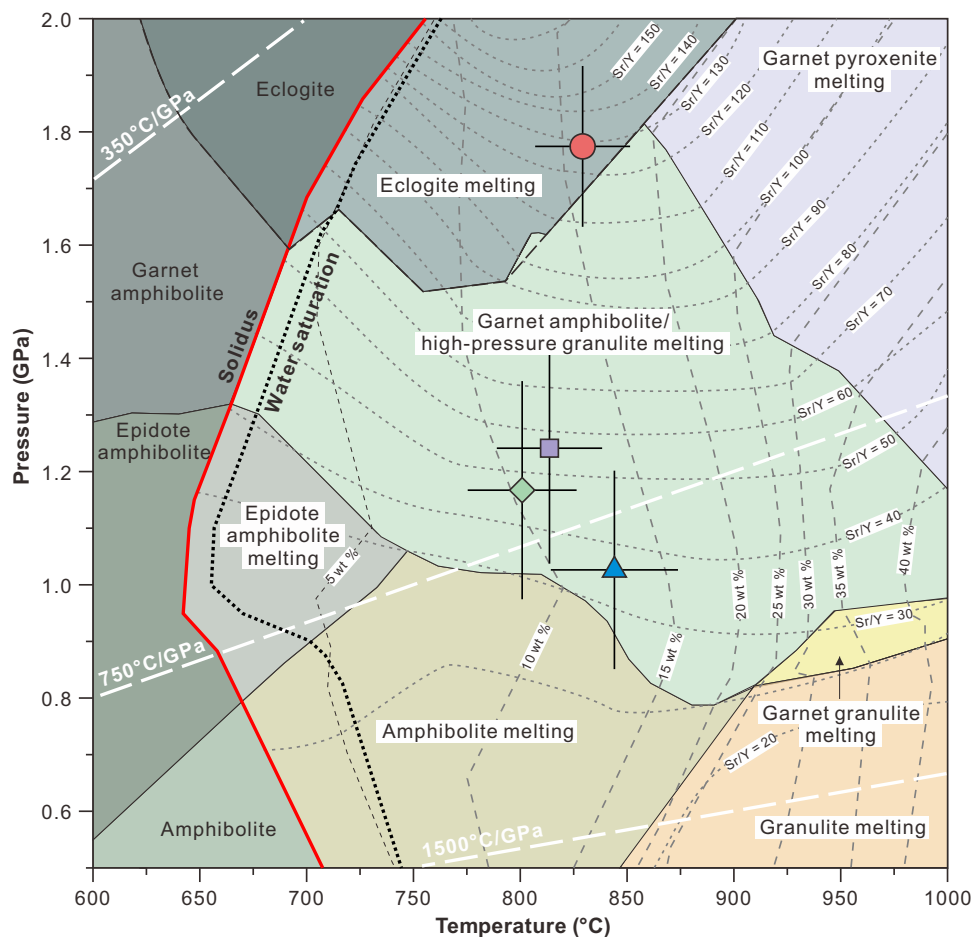
Fig. 5. Thermodynamic modeling. Simplified P-T phase diagram for the median Archean arc-like basalt (table S7), calculated with $X(H_2O) = 2.0$ wt %, corresponding to at least 0.3 wt % water-fluxed melting. Long and short dashed lines show calculated degree of melting (weight % of melt) and melt Sr/Y ratios, respectively. Dotted line marks water saturation of the system. Also shown are P-T conditions estimated for the Aktash tonalitic gneisses (red dot), compared to those for the Itsaq (purple square), Anshan (green diamond), and Acasta (group 2, blue triangle) TTG gneisses. Error bars are 1σ based on uncertainties in observed Sr/Y ratios, Sr contents (for pressure), and LILE contents (for degree of melting and temperature) and should be considered as minimum estimates. Whereas most Eoarchean TTGs were likely derived from thickened lower crust (1.0 to 1.5 GPa), the composition of the Aktash tonalites (for example, Sr/Y ≥ 100) requires melting at mantle depths (>1.6 GPa).

a relatively steep subduction angle, in contrast to flat subduction commonly assumed for the Archean (*2*, *38*). All these arguments suggest that modern-style arc subduction-accretion tectonics occurred, at least locally, at ~3.7 Ga. Our findings thus support the view of Eoarchean continental crust formation mainly by accretion of proto arcs, through partial melting of either thickened lower crust (*11*, *12*, *16*) or subducted arcs (this study). These processes, along with AFC in Iceland-like settings (*18*), built the oldest continental nuclei on Earth, upon which later crustal growth and reworking, through both subduction- and plume-related processes, continued to make more evolved and extensive continental crust.

MATERIALS AND METHODS
Field mapping and sampling
The outcrop was first mapped according to lithologies. Each lithology was sampled for laser ablation inductively coupled plasma mass spectrometry (LA-ICPMS) zircon dating, and one tonalitic gneiss (15ALT10) was found to be Eoarchean. Similar tonalitic gneisses around this sample

site were then sampled every ~2 m across and along the foliation, and selected samples were dated using a sensitive high-resolution ion microprobe (SHRIMP) to confirm ages and to constrain the exposed area of Eoarchean rocks. These dated samples, along with additional samples collected along the foliation at the same site, were used for whole-rock major and trace element analyses. All the samples were collected from relatively low-strain domains between major shear surfaces, and visible leucosomes or melt patches were carefully avoided during sampling.

In situ zircon U-Pb dating
Zircons were separated using standard density and magnetic techniques. They were handpicked and mounted in epoxy resin under a binocular microscope (along with standard zircon BR266) and polished to expose the central parts of the grains. Polished mounts were imaged by reflected and transmitted light and by CL. CL imaging was carried out at the Electron Microscopy and Microanalysis Facility, Curtin University, using a MIRA3 scanning electron microscope equipped with a monochromatic CL detector.

In situ zircon U-Th-Pb analyses were carried out by both SIMS and laser ablation. SIMS dating was performed using a SHRIMP II ion microprobe at Curtin University, following the standard procedures described in the study of De Laeter and Kennedy (47). A primary O^{2-} ion beam with intensity of ~2 nA and spot size of ~25 μm was used. Each analysis site was rastered for 120 s to remove surface contamination. Six scans through the nine mass stations were made for each spot analysis. Standard zircon BR266 ($^{206}Pb/^{238}U$ age = 559 Ma, U = 909 ppm) was analyzed before every three to four unknowns to calibrate measured Pb/U isotopic ratios and element concentrations. The assigned 1σ external error of Pb/U ratio for the standard zircons was between 0.5 and 1.4% during this study. Common lead was corrected using the measured ^{204}Pb and the present-day common lead composition given by (48). Data reduction was performed using SQUID 2.5 (49).

Laser ablation dating was carried out using the LA-ICPMS at the State Key Laboratory for Mineral Deposits Research, Nanjing University. A New Wave 193-nm laser-ablation system with an in-house sample cell coupled to an Agilent 7500s ICP-MS was used for U-Th-Pb isotopic analysis. All analyses were conducted using a beam diameter of 25 μm, a repetition rate of 5 Hz, and energy of 10 to 20 J/cm². Detailed instrumental setting and analytical procedures follow the methods outlined in the study of Jackson et al. (50). Mass discrimination and residual elemental fractionation were calibrated against the standard zircon GEMOC/GJ-1 ($^{206}Pb/^{238}U$ age of 601 Ma). Samples were analyzed in "runs" of about 15 analyses, which included 10 unknowns, bracketed at the beginning and the end by two analyses of the standard. The standard zircon Mud Tank was analyzed as an unknown in each run, and the weighted mean $^{206}Pb/^{238}U$ age was 727.8 ± 3.9 Ma (2σ, MSWD = 1.6, n = 55) during the analytical sessions, consistent with previous results in other laboratories (50). U-Pb ages were calculated using the online software package GLITTER (v. 4.4; www.glitter-gemoc.com/).

In situ zircon Lu-Hf isotopic analysis

Zircon Lu-Hf isotopic analyses were carried out at the State Key Laboratory for Mineral Deposits Research, Nanjing University, using a Neptune MC-ICP-MS equipped with a New Wave Research UP193-FX laser ablation system. The analytical procedures follow those described in the study of Wu et al. (51). The analyses were conducted with a repetition rate of 6 to 8 Hz, energy of 10 to 15 J/cm², and beam diameter of 32 or 44 μm. The raw counts of ^{172}Yb, ^{173}Yb, ^{175}Lu, $^{176}(Hf + Yb + Lu)$, ^{177}Hf, ^{178}Hf, ^{179}Hf, and ^{180}Hf were collected. The isobaric interference and instrumental mass bias were corrected using the methods and parameters given in the study of Wu et al. (51). Standard zircons Mud Tank, 91500, and Penglai were used to monitor the instrumental state and analytical accuracy. The resultant $^{176}Hf/^{177}Hf$ during the analyses was 0.282504 ± 0.000029 (2σ, n = 58) for Mud Tank, 0.282306 ± 0.000046 (2σ, n = 50) for 91500, and 0.282926 ± 0.000057 (2σ, n = 6) for Penglai. The εHf(t) was calculated using the chondrite parameter of $^{176}Hf/^{177}Hf = 0.282785$ and $^{176}Lu/^{177}Hf = 0.0336$ (52) and the ^{176}Lu decay constant of 1.867×10^{-11} (53). The 2SE error of εHf(t) was estimated following the methods given in the study of Ickert (54), whereas the 2σ errors of $^{176}Hf/^{177}Hf$ ratios and εHf(t) were calculated by quadratic addition of the internal error (2 SE) and the external reproducibility of the standard zircon Mud Tank (0.000029 or 1.0 ε unit). Careful optical and CL examination after Lu-Hf analysis reveals that several spots (15ALT10-39, 15ALT10-5.1, 16ALT04-12.1, 16ALT05-2.1, 16ALT05-6.3, 16ALT08-9.1, 16ALT08-10.2, and 16ALT08-15.1), mostly with exceptionally high $^{176}Hf/^{177}Hf$, were located on mixed zircon domains and were excluded from further interpretation.

Whole-rock geochemical analysis

Thirteen samples were pulverized to less than 200 mesh in an agate shatterbox. Major elements were determined by ARL-9900 x-ray fluorescence at the Shandong Bureau of China Metallurgical Geology Bureau (SBCMGB), Ji'nan, with precision and accuracy better than 5% (table S5). Trace element contents were analyzed using an X Series 2 ICP-MS at SBCMGB. To evaluate the accuracy of the data, we reanalyzed most samples using an Agilent 7700e ICP-MS at the China University of Geosciences, Wuhan. Sample digestion follows similar procedures in both laboratories (55), which are briefly described below. Sample powder was dried at 105°C for 12 hours in an oven, and dried powder was precisely weighted to a Teflon bomb. HNO_3 and Hf were added to the bomb to dissolve the powder by heating at 190°C (more than 24 hours) and drying at 140°C for three times. The power was completely dissolved in the acid, and no residue was found in the final solution. The analytical precision (relative SD) and accuracy (relative error to recommended values) based on multiple analyses of the standard materials AGV-2, BHVO-2, BCR-2, RGM-2, GSR-1, and GSR-3 are better than 10% for most (20% for all) trace elements in both laboratories (table S5). Replicate analyses on unknowns in each laboratory yielded similar precision to the standards. Comparison of sample data from the two laboratories suggests that inter-laboratory discrepancy is within 10% for most elements (table S5), except for Li, Sc, Sn, Cs, Tl, U, and Ta. High inter-laboratory discrepancies for Li and Sc may have resulted from contamination and polyatomic interference, respectively, whereas the apparent discrepancies for Sn, Cs, Ta, Tl, and U resulted from very low concentrations (thus high analytical uncertainties) of these elements in most of our samples [for example, Sn, Cs, and Tl (<0.5 ppm), U (<0.2 ppm), and Ta (<0.1 ppm); table S4]. While the low U (Cs and Th) concentrations probably resulted from mobilization during granulite facies metamorphism and were not used in the interpretations, Ta shows good positive correlation with Nb (fig. S5), suggesting that it was not significantly mobilized. However, the extremely low Ta contents impart extremely high Nb/Ta ratios (>30) probably with high analytical uncertainties; thus, we calculate Nb/Ta ratios only for samples with average Ta ≥ 0.1 ppm.

Data compilation

The TTG database used in this study was from Moyen (13), which is supplemented by literature data for Eoarchean (≥3.6 Ga) TTGs from the Itsaq, Acasta, and Anshan gneiss complexes (see table S4 for reference list). Eoarchean samples not assigned as TTGs or with SiO_2 < 56 wt % or K_2O/Na_2O > 1 were excluded. This, together with the Aktash data presented in this study, results in a database with 122 samples. It appears that TTGs from each Eoarchean gneiss complex have distinct geochemical compositions, probably due to derivation from different depths, although considerable variations exist in each suite due to fractionation and/or mixing of melts derived from different depths. The mean, median, and SD of each suite were calculated, and median values were used for trace element modeling.

To evaluate the source composition and tectonic setting of Archean TTGs, we compiled databases for mafic volcanic rocks from Archean cratons and modern mid-ocean ridges, oceanic plateaus, and oceanic arcs from the GEOROC and/or PetDB databases. Data for Archean cratons and modern oceanic arcs are from GEOROC (http://georoc. mpch-mainz.gwdg.de/georoc/; accessed in April and June 2016, respectively). Data for modern oceanic plateaus were also from GEOROC and were supplemented by oceanic plateau data from PetDB (www.earthchem. org/petdb). Data for the mid-ocean ridge basalts were from PetDB. All

the databases were filtered using the following procedures: (i) being volcanic rock or glass; (ii) SiO_2 between 42 to 56 wt %, and MgO <18 wt %; and (iii) LOI (loss on ignition) < 5 wt % or sum of major elements within 97 to 103 wt %. Furthermore, data beyond the 2σ range of the original data were excluded, and the mean, median, and SD were recalculated. The Archean basalts were further filtered with Th/Nb > 0.1 (27) to identify those with arc-like trace element patterns (that is, negative Nb-Ta anomalies). Note that these arc-like basalts did not necessarily form in arcs because continental contamination is difficult to exclude (27). However, the resultant average composition is an appropriate source for TTGs in terms of LILE enrichment and appears to be representative of the least altered, Eoarchean high-Al tholeiites from the Isua and Nuvvuagittuq greenstone belts that were interpreted to have formed in Eoarchean proto-arcs (30–35).

Thermodynamic and trace element partial melting modeling

Thermodynamic partial melting modeling was carried out with Perple_X (56) (version 6.7.6) in the $Na_2O\text{-}CaO\text{-}K_2O\text{-}FeO\text{-}MgO\text{-}Al_2O_3\text{-}SiO_2\text{-}H_2O\text{-}TiO_2\text{-}O_2$ system, using the thermodynamic database from Holland and Powell (57) (hp622ver.dat) and the newly calibrated solution models for tonalitic melt [melt(G)], amphibole [cAmph(G)], and clinopyroxene [Augite(G)] from Green et al. (36). Other solution models used in the calculation included Gt(W) for garnet (58), Opx(W) for orthopyroxene (58), Ilm(WPH) for ilmenite (58), Bi(W) for biotite (58), Chl(W) for chlorite (58), and Mica(W) for mica (58), Fsp(C1) for plagioclase (59), and Ep (HP11) for epidote (57). Quartz, rutile, sphene (titanite), and water were considered as pure end-members. The calculation was performed for the median composition of Archean arc-like basalts (table S7), assuming a $Fe^{3+}/(Fe^{3+} + Fe^{2+})$ ratio of 0.1. The P-T phase diagram was calculated with 2 and 1 wt % water, corresponding to water saturated and water undersaturated melting, respectively, at 1.0 GPa (fig. S8). Equilibrium mineral assemblages were also calculated at discrete P-T points for every 10°C and 0.1 GPa from 750° to 950°C and 0.6 to 2.0 GPa, with a water content of 1.0, 1.5, 2.0, 2.5, and 3.0 wt %, respectively (table S9). The resultant weight percentages of melts and the equilibrium minerals were then used to calculate the trace element composition of the melts.

Trace element modeling was carried out using the batch melting equation (60)

$$C_{melt}/C_{source} = 1/[D + F*(1-D)]$$

where C_{source} and C_{melt} represent concentration of a trace element in the source rock and the resultant melt, respectively; D is the bulk partition coefficient, and F is the degree of melting (that is, weight % of melt). The median values of the mafic source rocks were used, and the results were compared with the median values of TTGs, because the distribution of most elements in these large databases were skewed and the means were biased by high values (fig. S8). Partition coefficients (table S8) were mostly cited from Bédard (8), except for those for garnet and plagioclase from Qian and Hermann (37), and Nb, Ta, and Ti data for rutile from Xiong et al. (40). The garnet REE and Y partition coefficients we used were lower than those given by Bédard (8); use of higher values resulted in a poorer fit of heavy REE slope with the target TTG composition. The D value for Sr in plagioclase we used (2.262) was also lower than that given in the study of Bédard (8) (6.65), so that the resultant melt Sr content is less sensitive to the amount of residual plagioclase.

SUPPLEMENTARY MATERIALS

Supplementary Text
fig. S1. Regional geological setting of the Aktash gneiss complex.
fig. S2. Field photographs of the Eoarchean Aktash tonalitic gneisses and related rocks.
fig. S3. Photomicrographs of the Eoarchean tonalitic gneisses and associated rocks.
fig. S4. Concordia diagrams and representative zircon CL images of the Eoarchean tonalitic gneisses.
fig. S5. Binary element variation diagrams of the Aktash tonalites.
fig. S6. REE and trace element patterns for the Eoarchean TTG gneisses.
fig. S7. Histograms of LILEs (for example, K, Rb, Ba, and Th).
fig. S8. Phase diagrams calculated for the median composition of Archean arc-like basalts.
fig. S9. Trace element patterns of modeled melts compared to the Eoarchean TTGs from the Itsaq, Anshan, and Acasta complexes.
fig. S10. Zircon saturation temperature (T_{Zr}).
table S1. SHRIMP zircon U-Th-Pb isotopic data for the Eoarchean gneisses in the Aktash Tagh area, southeast Tarim Craton, northwestern China.
table S2. LA-ICPMS zircon ages for the Eoarchean gneisses in the Aktash Tagh area, southeast Tarim Craton, northwestern China.
table S3. LA-MC-ICPMS zircon Lu-Hf isotopic data for the Eoarchean gneisses in the Aktash Tagh area, southeast Tarim Craton, northwestern China.
table S4. Whole-rock geochemical data for the Eoarchean tonalitic gneisses in the Aktash Tagh area, southeast Tarim Craton, northwestern China, and literature data for the Eoarchean TTGs from the Itsaq, Acasta, and Anshan gneiss complexes.
table S5. Major and trace element composition of standard materials analyzed along with unknowns during this study.
table S6. Average composition of TTGs for different ages and assumed melting pressures.
table S7. Average composition of potential source mafic rocks for Archean TTGs compiled from the GEOROC and PetDB databases.
table S8. Mineral partition coefficients used in trace element modeling of partial melting of mafic rocks [after Bédard (8) and Martin et al. (7)].
table S9. Thermodynamic and trace element modeling of partial melting of median Archean arc-like basalt.
References (61–73)

REFERENCES AND NOTES

1. J.-F. Moyen, H. Martin, Forty years of TTG research. Lithos 148, 312–336 (2012).
2. K. C. Condie, How to make a continent: Thirty-five years of TTG research, in Evolution of Archean Crust and Early Life, Y. Dilek, H. Furnes, Eds (Springer, 2014), pp. 179–193.
3. H. Martin, R. H. Smithies, R. Rapp, J.-F. Moyen, D. Champion, An overview of adakite, tonalite–trondhjemite–granodiorite (TTG), and sanukitoid: Relationships and some implications for crustal evolution. Lithos 79, 1–24 (2005).
4. O. Laurent, H. Martin, J. F. Moyen, R. Doucelance, The diversity and evolution of late-Archean granitoids: Evidence for the onset of "modern-style" plate tectonics between 3.0 and 2.5 Ga. Lithos 205, 208–235 (2014).
5. H. Martin, Effect of steeper Archean geothermal gradient on geochemistry of subduction-zone magmas. Geology 14, 753–756 (1986).
6. M. S. Drummond, M. J. Defant, A model for trondhjemite-tonalite-dacite genesis and crustal growth via slab melting: Archean to modern comparisons. J. Geophys. Res. 95, 21503–21521 (1990).
7. H. Martin, J.-F. Moyen, M. Guitreau, J. Blichert-Toft, J.-L. Le Pennec, Why Archaean TTG cannot be generated by MORB melting in subduction zones. Lithos 198–199, 1–13 (2014).
8. J. H. Bédard, A catalytic delamination-driven model for coupled genesis of Archaean crust and sub-continental lithospheric mantle. Geochim. Cosmochim. Acta 70, 1188–1214 (2006).
9. R. H. Smithies, D. C. Champion, M. J. Van Kranendonk, Formation of Paleoarchean continental crust through infracrustal melting of enriched basalt. Earth Planet. Sci. Lett. 281, 298–306 (2009).
10. T. E. Johnson, M. Brown, N. J. Gardiner, C. L. Kirkland, R. H. Smithies, Earth's first stable continents did not form by subduction. Nature 543, 239–242 (2017).
11. T. J. Nagel, J. E. Hoffmann, C. Münker, Generation of Eoarchean tonalite-trondhjemite-granodiorite series from thickened mafic arc crust. Geology 40, 375–378 (2012).
12. J. E. Hoffmann, T. J. Nagel, C. Münker, T. Næraa, M. T. Rosing, Constraining the process of Eoarchean TTG formation in the Itsaq Gneiss Complex, southern West Greenland. Earth Planet. Sci. Lett. 388, 374–386 (2014).
13. J. Moyen, The composite Archaean grey gneisses: Petrological significance, and evidence for a non-unique tectonic setting for Archaean crustal growth. Lithos 123, 21–36 (2011).

14. A. P. Nutman, V. C. Bennett, C. R. L. Friend, Proposal for a continent 'Itsaqia' amalgamated at 3.66 Ga and rifted apart from 3.53 Ga: Initiation of a Wilson Cycle near the start of the rock record. *Am. J. Sci.* **315**, 509–536 (2015).

15. A. P. Nutman, V. C. Bennett, C. R. L. Friend, K. Horie, H. Hidaka, ~3,850 Ma tonalites in the Nuuk region, Greenland: Geochemistry and their reworking within an Eoarchaean gneiss complex. *Contrib. Mineral. Petrol.* **154**, 385–408 (2007).

16. J. E. Hoffmann, C. Münker, T. Næraa, M. T. Rosing, D. Herwartz, D. Garbe-Schönberg, H. Svahnberg, Mechanisms of Archean crust formation inferred from high-precision HFSE systematics in TTGs. *Geochim. Cosmochim. Acta* **75**, 4157–4178 (2011).

17. S. J. Mojzsis, N. L. Cates, G. Caro, D. Trail, O. Abramov, M. Guitreau, J. Blichert-Toft, M. D. Hopkins, W. Bleeker, Component geochronology in the polyphase ca. 3920 Ma Acasta gneiss. *Geochim. Cosmochim. Acta* **133**, 68–96 (2014).

18. J. R. Reimink, T. Chacko, R. A. Stern, L. M. Heaman, Earth's earliest evolved crust generated in an Iceland-like setting. *Nat. Geosci.* **7**, 529–533 (2014).

19. Y. Wan, D. Liu, A. Nutman, H. Zhou, C. Dong, X. Yin, M. Ma, Multiple 3.8–3.1 Ga tectono-magmatic events in a newly discovered area of ancient rocks (the Shengousi Complex), Anshan, North China Craton. *J. Asian Earth Sci.* **54–55**, 18–30 (2012).

20. Y.-F. Wang, X.-H. Li, W. Jin, J.-H. Zhang, Eoarchean ultra-depleted mantle domains inferred from ca. 3.81 Ga Anshan trondhjemitic gneisses, North China Craton. *Precambrian Res.* **263**, 88–107 (2015).

21. S. Lu, H. Li, C. Zhang, G. Niu, Geological and geochronological evidence for the Precambrian evolution of the Tarim Craton and surrounding continental fragments. *Precambrian Res.* **160**, 94–107 (2008).

22. J. Hiess, V. C. Bennett, Chondritic Lu/Hf in the early crust–mantle system as recorded by zircon populations from the oldest Eoarchean rocks of Yilgarn Craton, West Australia and Enderby Land, Antarctica. *Chem. Geol.* **427**, 125–143 (2016).

23. O. Jagoutz, M. W. Schmidt, A. Enggist, J.-P. Burg, D. Hamid, S. Hussain, TTG-type plutonic rocks formed in a modern arc batholith by hydrous fractionation in the lower arc crust. *Contrib. Mineral. Petrol.* **166**, 1099–1118 (2013).

24. A. C. Kerr, Oceanic plateaus, in *Treatise on Geochemistry*, R. L. Rudnick, Ed. (Elsevier, 2014), vol. 4, pp. 631–667.

25. A. R. Hastie, J. G. Fitton, G. D. Bromiley, I. B. Butler, N. W. A. Odling, The origin of Earth's first continents and the onset of plate tectonics. *Geology* **44**, 855–858 (2016).

26. T. W. Sisson, K. Ratajeski, W. B. Hankins, A. F. Glazner, Voluminous granitic magmas from common basaltic sources. *Contrib. Mineral. Petrol.* **148**, 635–661 (2005).

27. J. A. Pearce, Geochemical fingerprinting of oceanic basalts with applications to ophiolite classification and the search for Archean oceanic crust. *Lithos* **100**, 14–48 (2008).

28. C. Herzberg, K. Condie, J. Korenaga, Thermal history of the Earth and its petrological expression. *Earth Planet. Sci. Lett.* **292**, 79–88 (2010).

29. T. E. Johnson, M. Brown, B. J. P. Kaus, J. A. VanTongeren, Delamination and recycling of Archaean crust caused by gravitational instabilities. *Nat. Geosci.* **7**, 47–52 (2014).

30. J. E. Hoffmann, C. Münker, A. Polat, M. T. Rosing, T. Schulz, The origin of decoupled Hf–Nd isotope compositions in Eoarchean rocks from southern West Greenland. *Geochim. Cosmochim. Acta* **75**, 6610–6628 (2011).

31. F. E. Jenner, V. C. Bennett, A. P. Nutman, C. R. L. Friend, M. D. Norman, G. Yaxley, Evidence for subduction at 3.8 Ga: Geochemistry of arc-like metabasalts from the southern edge of the Isua Supracrustal Belt. *Chem. Geol.* **261**, 83–98 (2009).

32. A. Polat, A. W. Hofmann, Alteration and geochemical patterns in the 3.7–3.8 Ga Isua greenstone belt, West Greenland. *Precambrian Res.* **126**, 197–218 (2003).

33. S. Turner, T. Rushmer, M. Reagan, J.-F. Moyen, Heading down early on? Start of subduction on Earth. *Geology* **42**, 139–142 (2014).

34. A. P. Nutman, V. C. Bennett, C. R. L. Friend, The emergence of the Eoarchaean proto-arc: Evolution of a *c.* 3700 Ma convergent plate boundary at Isua, southern West Greenland. *Geol. Soc. Spec. Publ.* **389**, 113–133 (2014).

35. J. Adam, T. Rushmer, J. O'Neil, D. Francis, Hadean greenstones from the Nuvvuagittuq fold belt and the origin of the Earth's early continental crust. *Geology* **40**, 363–366 (2012).

36. E. C. R. Green, R. W. White, J. F. A. Diener, R. Powell, T. J. B. Holland, R. M. Palin, Activity–composition relations for the calculation of partial melting equilibria in metabasic rocks. *J. Metamorph. Geol.* **34**, 845–869 (2016).

37. Q. Qian, J. Hermann, Partial melting of lower crust at 10–15 kbar: Constraints on adakite and TTG formation. *Contrib. Mineral. Petrol.* **165**, 1195–1224 (2013).

38. R. M. Palin, R. W. White, E. C. R. Green, Partial melting of metabasic rocks and the generation of tonalitic–trondhjemitic–granodioritic (TTG) crust in the Archaean: Constraints from phase equilibrium modelling. *Precambrian Res.* **287**, 73–90 (2016).

39. R. P. Rapp, M. D. Norman, D. Laporte, G. M. Yaxley, H. Martin, S. F. Foley, Continent formation in the Archean and chemical evolution of the cratonic lithosphere: Melt–rock reaction experiments at 3–4 GPa and petrogenesis of Archean Mg-diorites (Sanukitoids). *J. Petrol.* **51**, 1237–1266 (2010).

40. X. Xiong, H. Keppler, A. Audétat, H. Ni, W. Sun, Y. Li, Partitioning of Nb and Ta between rutile and felsic melt and the fractionation of Nb/Ta during partial melting of hydrous metabasalt. *Geochim. Cosmochim. Acta* **75**, 1673–1692 (2011).

41. M. Brown, Duality of thermal regimes is the distinctive characteristic of plate tectonics since the Neoarchean. *Geology* **34**, 961–964 (2006).

42. S. B. Shirey, S. H. Richardson, Start of the Wilson cycle at 3 Ga shown by diamonds from subcontinental mantle. *Science* **333**, 434–436 (2011).

43. B. Dhuime, C. J. Hawkesworth, P. A. Cawood, C. D. Storey, A change in the geodynamics of continental growth 3 billion years ago. *Science* **335**, 1334–1336 (2012).

44. T. Naeraa, A. Scherstén, M. T. Rosing, A. Kemp, J. E. Hoffmann, T. F. Kokfelt, M. J. Whitehouse, Hafnium isotope evidence for a transition in the dynamics of continental growth 3.2 Gyr ago. *Nature* **485**, 627–630 (2012).

45. M. Tang, K. Chen, R. L. Rudnick, Archean upper crust transition from mafic to felsic marks the onset of plate tectonics. *Science* **351**, 372–375 (2016).

46. E. Sizova, T. Gerya, M. Brown, L. L. Perchuk, Subduction styles in the Precambrian: Insight from numerical experiments. *Lithos* **116**, 209–229 (2010).

47. J. R. De Laeter, A. K. Kennedy, A double focusing mass spectrometer for geochronology. *Int. J. Mass Spectrom.* **178**, 43–50 (1998).

48. J. S. Stacey, J. D. Kramers, Approximation of terrestrial lead isotope evolution by a two-stage model. *Earth Planet. Sci. Lett.* **26**, 207–221 (1975).

49. K. Ludwig, SQUID 2: A User's Manual. *Berkeley Geochronology Centre Spec. Pub.* **5**, 1–110 (2009).

50. S. E. Jackson, N. J. Pearson, W. L. Griffin, E. A. Belousova, The application of laser ablation-inductively coupled plasma-mass spectrometry to in situ U–Pb zircon geochronology. *Chem. Geol.* **211**, 47–69 (2004).

51. F.-Y. Wu, Y.-H. Yang, L.-W. Xie, J.-H. Yang, P. Xu, Hf isotopic compositions of the standard zircons and baddeleyites used in U–Pb geochronology. *Chem. Geol.* **234**, 105–126 (2006).

52. A. Bouvier, J. D. Vervoort, P. J. Patchett, The Lu–Hf and Sm–Nd isotopic composition of CHUR: Constraints from unequilibrated chondrites and implications for the bulk composition of terrestrial planets. *Earth Planet. Sci. Lett.* **273**, 48–57 (2008).

53. U. Söderlund, P. J. Patchett, J. D. Vervoort, C. E. Isachsen, The ^{176}Lu decay constant determined by Lu–Hf and U–Pb isotope systematics of Precambrian mafic intrusions. *Earth Planet. Sci. Lett.* **219**, 311–324 (2004).

54. R. B. Ickert, Algorithms for estimating uncertainties in initial radiogenic isotope ratios and model ages. *Chem. Geol.* **340**, 131–138 (2013).

55. Y. Liu, K. Zong, P. B. Kelemen, S. Gao, Geochemistry and magmatic history of eclogites and ultramafic rocks from the Chinese continental scientific drill hole: Subduction and ultrahigh-pressure metamorphism of lower crustal cumulates. *Chem. Geol.* **247**, 133–153 (2008).

56. J. A. D. Connolly, Computation of phase equilibria by linear programming: A tool for geodynamic modeling and its application to subduction zone decarbonation. *Earth Planet. Sci. Lett.* **236**, 524–541 (2005).

57. T. J. B. Holland, R. Powell, An improved and extended internally consistent thermodynamic dataset for phases of petrological interest, involving a new equation of state for solids. *J. Metamorph. Geol.* **29**, 333–383 (2011).

58. R. W. White, R. Powell, T. E. Johnson, The effect of Mn on mineral stability in metapelites revisited: New *a–x* relations for manganese-bearing minerals. *J. Metamorph. Geol.* **32**, 809–828 (2014).

59. T. Holland, R. Powell, Activity–composition relations for phases in petrological calculations: An asymmetric multicomponent formulation. *Contrib. Mineral. Petrol.* **145**, 492–501 (2003).

60. D. M. Shaw, Trace element fractionation during anatexis. *Geochim. Cosmochim. Acta* **34**, 237–243 (1970).

61. R. F. Ge, W. B. Zhu, S. A. Wilde, H. L. Wu, J. W. He, B. H. Zheng, Archean magmatism and crustal evolution in the northern Tarim Craton: Insights from zircon U–Pb–Hf–O isotopes and geochemistry of ~2.7 Ga orthogneiss and amphibolite in the Korla Complex. *Precambrian Res.* **252**, 145-165 (2014).

62. Xinjiang Bureau of Geology and Mineral Resources, *Regional geology of Xinjiang Uygur Autonomy Region*, 762 (Geological Publishing House, 1993).

63. X. P. Long, C. Yuan, M. Sun, A. Kröner, G. Zhao, New geochemical and combined zircon U–Pb and Lu–Hf isotopic data of orthogneisses in the northern Altyn Tagh, northern margin of the Tibetan plateau: Implication for Archean evolution of the Dunhuang Block and crust formation in NW China. *Lithos* **200–203**, 418–431 (2014).

64. H. T. Xin, Y. S. Liu, Z. H. Luo, S. C. Song, S. Q. Wang, The growth of Archean continental crust in Aqtashtagh Area of Southeast Tarim, China: Constraints from petrochemistry and chronology about Milan Group and TTG-gneiss. *Earth Sci. Front.* **20**, 240–259 (2013).

65. H. T. Xin, F. Q. Zhao, Z. Luo, Y. S. Liu, Y. S. Wan, S. Q. Wang, Determination of the Paleoproterozoic geochronological framework in Aqtashtagh area in Southeastern Tarim, China, and its geological significance. *Acta Geol. Sin.* **85**, 1977–1993 (2011).

66. C.-L. Zhang, H.-B. Zou, M. Santosh, X.-T. Ye, H.-K. Li, Is the Precambrian basement of the Tarim Craton in NW China composed of discrete terranes? *Precambrian Res.* **254**, 226–244 (2014).

67. G. E. Gehrels, A. Yin, X.-F. Wang, Magmatic history of the northeastern Tibetan Plateau. *J. Geophys. Res.* **108**, 2423 (2003).

68. Y. Zhao, C. R. Diwu, W. H. Ao, H. L. Wang, T. Zhu, Y. Sun, Ca. 3.06 Ga granodioritic gneiss in Dunhuang block. *Chinese Sci. Bull.* **60**, 75–38 (2015).

69. H. Y. Xin, Z. H. Luo, Y. S. Liu, S. Q. Wang, Z. L. Zhang, Geological features and significance of Paleoproterozoic carbonatite of crust origin in Aqtashtagh area of southeast Tarim Basin, China. *Earth Sci. Front.* **6**, 167–178 (2012).

70. H.-M. Li, S.-N. Lu, J.-K. Zheng, H.-F. Yu, F.-Q. Zhao, H.-K. Li, Y.-C. Zou, Dating of 3.6 Ga zircons in granite-gneiss from the eastern Altyn Mountains and its geological significance. *Bull. Mineral. Petrol. Geochem.* **20**, 259–262 (2001).

71. D. A. Wyman, J. A. Ayer, J. R. Devaney, Niobium-enriched basalts from the Wabigoon subprovince, Canada: Evidence for adakitic metasomatism above an Archean subduction zone. *Earth Planet. Sci. Lett.* **179**, 21–30 (2000).

72. A. Polat, A. W. Hofmann, M. T. Rosing, Boninite-like volcanic rocks in the 3.7–3.8 Ga Isua greenstone belt, West Greenland: Geochemical evidence for intra-oceanic subduction zone processes in the early Earth. *Chem. Geol.* **184**, 231–254 (2002).

73. C. G. Macpherson, S. T. Dreher, M. F. Thirlwall, Adakites without slab melting: High pressure differentiation of island arc magma, Mindanao, the Philippines. *Earth Planet. Sci. Lett.* **243**, 581–593 (2006).

Science Advances

Remnants of Eoarchean continental crust derived from a subducted proto-arc

Rongfeng Ge, Wenbin Zhu, Simon A. Wilde and Hailin Wu

ARTICLE TOOLS	http://advances.sciencemag.org/content/4/2/eaao3159
SUPPLEMENTARY MATERIALS	http://advances.sciencemag.org/content/suppl/2018/02/12/4.2.eaao3159.DC1
REFERENCES	This article cites 70 articles, 10 of which you can access for free http://advances.sciencemag.org/content/4/2/eaao3159#BIBL
PERMISSIONS	http://www.sciencemag.org/help/reprints-and-permissions

Use of this article is subject to the Terms of Service